Supporting Information

Homochiral Dy_2 single-molecule magnets with strong magneto-optical Faraday effect and strong third-harmonic generation

Cai-Ming Liu*[a], Rong Sun[b], Xiang Hao[a], Xi-Li Li[c] and Bing-Wu Wang*[c]

[a] *Beijing National Laboratory for Molecular Sciences, CAS Key Laboratory for Organic Solids, Institute of Chemistry, Chinese Academy of Sciences, Beijing 100190, China. Email: cmliu@iccas.ac.cn*

[b] *State Key Laboratory of Rare Earth Materials Chemistry and Applications, College of Chemistry and Molecular Engineering, Peking University, Beijing 100871, China.* Email: wangbw@pku.edu.cn

[c] *Henan Provincial Key Laboratory of Surface and Interface Science, Zhengzhou University of Light Industry, Zhengzhou 450002, China.*

Contents

12. Tables S6-S9. Calculated energy levels and $g(g_x, g_y, g_z)$ tensors of the lowest Kramers doublets (KDs) of individual Dy(III) fragment for *D*-**1**, *D*-**2**, *D*-**3** and *D*-**4**.
13. Tables S10- S13. Wave functions with definite projection of the total moment $|m_J>$ for the lowest three Kramers doublets (KDs) of individual Dy^{3+} fragments in *D*-**1**, *D*-**2**, *D*-**3** and *D*-**4**.
14. Fig. S13. Plots of χT *versus* T of *D*-**1**, *D*-**2**, *D*-**3** and *D*-**4** with the simulated results.
15. Figs. S14-S17. The orientations of easy axis of the KDs on Dy^{3+} for *D*-**1**, *D*-**2**, *D*-**3** and *D*-**4**.
16. Figs. S18-S21. MCD spectra of *D*-**1**/*L*-**1**, *D*-**2**/*L*-**2**, *D*-**3**/*L*-**3** and *D*-**4**/*L*-**4**.
17. Figs. S22-S25. The wavelength-dependent g_{MCD} curves of *D*-**1**/*L*-**1**, *D*-**2**/*L*-**2**, *D*-**3**/*L*-**3** and *D*-**4**/*L*-**4**.
18. Fig. S26. SHG spectra of crystalline samples of *D*-**1**, *D*-**2**, *D*-**3**, *D*-**4** and KDP (illustration) under excitation at λ = 1550 nm (T_{int} = 0.5 s).

Table S1. Crystal data and structural refinement parameters for *D*-**1**/*L*-**1**, *D*-**2**/*L*-**2**, *D*-**3**/*L*-**3**, *D*-**4**/*L*-**4**.

	D-**1**	*L*-**1**	*D*-**2**	*L*-**2**	*D*-**3**	*L*-**3**	*D*-**4**	*L*-**4**
formula	$C_{56}H_{68}F_6N_{10}O_{14}Dy_2$	$C_{56}H_{68}F_6N_{10}O_{14}Dy_2$	$C_{58}H_{70}Dy_2F_6N_8O_{14}$	$C_{58}H_{70}Dy_2F_6N_8O_{14}$	$C_{60}H_{62}Dy_2F_{14}N_{10}O_{12}$	$C_{60}H_{62}Dy_2F_{14}N_{10}O_{12}$	$C_{62}H_{69}Dy_2F_{14}N_8O_{14}$	$C_{62}H_{69}Dy_2F_{14}N_8O_{14}$
F_W	1544.20	1544.20	1542.22	1542.22	1706.19	1706.19	1741.25	1741.25
crystal system	monoclinic	monoclinic	monoclinic	monoclinic	triclinic	triclinic	monoclinic	monoclinic
space group	$P2_1$	$P2_1$	$P2_1$	$P2_1$	$P1$	$P1$	$P2_1$	$P2_1$
a[Å]	11.9091(2)	11.91880(16)	11.9571(2)	11.94360(18)	11.3419(2)	11.3542(2)	18.0384(5)	18.0064(4)
b[Å]	18.6155(2)	18.5949(3)	18.4949(3)	18.4933(3)	16.6925(3)	16.7025(3)	10.5248(2)	10.5352(2)
c[Å]	13.9636(2)	13.9673(2)	14.1630(2)	14.1704(2)	18.8529(4)	18.8605(4)	18.9442(5)	18.9592(4)
α[°]	90.00	90.00	90.00	90.00	70.521(2)	70.275(2)	90.00	90.00
β[°]	93.0150(10)	92.9810(12)	93.4050(10)	93.2910(14)	89.7460(10)	89.9510(10)	108.627(3)	108.460(2)
γ[°]	90.00	90.00	90.00	90.00	82.7060(10)	82.8120(10)	90.00	90.00
V[Å^3]	3091.36(8)	3091.37(8)	3126.55(9)	3124.75(8)	3335.05(12)	3337.16(12)	3408.17(16)	3411.52(13)
Z	2	2	2	2	2	2	2	2
ρ_{calc}[g cm^{-3}]	1.659	1.659	1.638	1.639	1.701	1.698	1.697	1.692
μ[mm^{-1}]	2.487	2.487	2.458	2.460	2.329	2.327	2.282	2.280
T[K]	170	170	170	170	170	170	170	170
λ [Å]	0.71073	0.71073	0.71073	0.71073	0.71073	0.71073	0.71073	0.71073
reflections collected	53168	53508	49359	62716	89540	89477	50504	46717
unique reflections	16564	16571	16769	16650	24878	24868	18259	12053
observed reflections	16145	15756	16048	15584	23781	22026	16389	11445
parameters	806	806	805	805	1700	1700	913	915
GoF[$I\geq2\sigma$ (I)]	1.024	1.047	1.016	1.027	1.068	1.030	1.045	1.035
R_1[$I\geq2\sigma$ (I)]	0.0177	0.0222	0.0211	0.0254	0.0628	0.0548	0.0398	0.0317
$_wR_2$[$I\geq2\sigma$ (I)]	0.0429	0.0526	0.0507	0.0598	0.1722	0.1455	0.1029	0.0804
Flack value	-0.007(2)	0.016(4)	-0.006(4)	-0.019(6)	0.018(17)	0.037(6)	0.011(7)	0.012(9)
CCDC	2308016	2308017	2308018	2308019	2308020	2308021	2308022	2308023

Table S2. Dy (III) ion geometry analysis by SHAPE 2.1 software for *D*-**1**.

Configuration	ABOXIY **Dy1**	ABOXIY **Dy2**
Octagon(D_{8h})	32.232	32.403
Heptagonal pyramid(C_{7v})	21.806	21.495
Hexagonal bipyramid(D_{6h})	11.660	12.296
Cube (O_h)	7.722	8.277
Square antiprism (D_{4d})	2.585	2.999
Triangular dodecahedron (D_{2d})	**1.726**	**1.487**
Johnson gyrobifastigium J26 (D_{2d})	12.057	12.518
Johnson elongated triangular bipyramid J14 (D_{3h})	26.094	26.098
Biaugmented trigonal prism J50 (C_{2v})	3.482	3.654
Biaugmented trigonal prism (C_{2v})	2.291	2.420
Snub diphenoid J84 (D_{2d})	5.024	4.685
Triakis tetrahedron (T_d)	8.591	9.072
Elongated trigonal bipyramid (D_{3h})	23.298	23.074

Table S3. Dy (III) ion geometry analysis by SHAPE 2.1 software for *D*-**2**.

Configuration	ABOXIY **Dy1**	ABOXIY **Dy2**
Octagon(D_{8h})	32.235	32.327
Heptagonal pyramid(C_{7v})	21.879	21.434
Hexagonal bipyramid(D_{6h})	11.763	12.297
Cube (O_h)	7.903	8.356
Square antiprism (D_{4d})	2.596	3.059
Triangular dodecahedron (D_{2d})	**1.784**	**1.530**
Johnson gyrobifastigium J26 (D_{2d})	11.944	12.438
Johnson elongated triangular bipyramid J14 (D_{3h})	26.665	26.256
Biaugmented trigonal prism J50 (C_{2v})	3.370	3.655
Biaugmented trigonal prism (C_{2v})	2.130	2.396
Snub diphenoid J84 (D_{2d})	5.106	4.719
Triakis tetrahedron (T_d)	8.745	9.157
Elongated trigonal bipyramid (D_{3h})	23.274	23.229

Table S4. Dy (III) ion geometry analysis by SHAPE 2.1 software for *D*-**3**.

Configuration	ABOXIY **Dy1**	ABOXIY **Dy2**	ABOXIY **Dy3**	ABOXIY **Dy4**
Octagon(D_{8h})	30.500	30.053	30.942	31.076
Heptagonal pyramid(C_{7v})	21.402	22.185	22.268	22.092
Hexagonal bipyramid(D_{6h})	14.775	14.809	14.455	12.365
Cube (O_h)	12.478	12.788	11.974	10.412
Square antiprism (D_{4d})	4.622	5.003	4.285	3.944
Triangular dodecahedron (D_{2d})	**2.589**	2.590	**2.406**	2.844
Johnson gyrobifastigium J26 (D_{2d})	11.770	11.154	10.884	10.337
Johnson elongated triangular bipyramid J14 (D_{3h})	22.146	21.740	22.250	22.052
Biaugmented trigonal prism J50 (C_{2v})	3.040	**2.589**	3.043	3.014
Biaugmented trigonal prism (C_{2v})	2.896	2.600	2.955	**2.564**
Snub diphenoid J84 (D_{2d})	3.463	3.058	2.888	3.525
Triakis tetrahedron (T_d)	13.269	13.587	12.746	11.224
Elongated trigonal bipyramid (D_{3h})	20.409	20.089	20.721	20.406

Table S5. Dy (III) ion geometry analysis by SHAPE 2.1 software for *D*-**4**.

Configuration	ABOXIY **Dy1**	ABOXIY **Dy2**
Octagon(D_{8h})	32.525	33.076
Heptagonal pyramid(C_{7v})	21.233	22.566
Hexagonal bipyramid(D_{6h})	10.882	10.357
Cube (O_h)	7.678	7.297
Square antiprism (D_{4d})	3.020	2.824
Triangular dodecahedron (D_{2d})	**2.193**	**2.365**
Johnson gyrobifastigium J26 (D_{2d})	11.150	10.941
Johnson elongated triangular bipyramid J14 (D_{3h})	25.509	26.361
Biaugmented trigonal prism J50 (C_{2v})	3.801	3.710
Biaugmented trigonal prism (C_{2v})	2.496	2.451
Snub diphenoid J84 (D_{2d})	5.605	6.007
Triakis tetrahedron (T_d)	8.541	8.098
Elongated trigonal bipyramid (D_{3h})	22.925	22.986

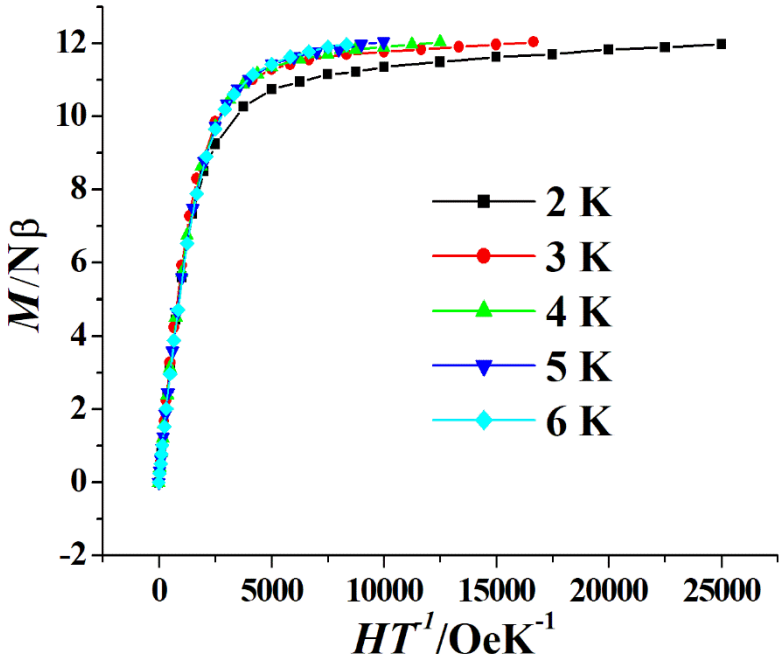

Fig. S1. *M versus H*/*T* plots at 2-6 K of *D*-**1**.

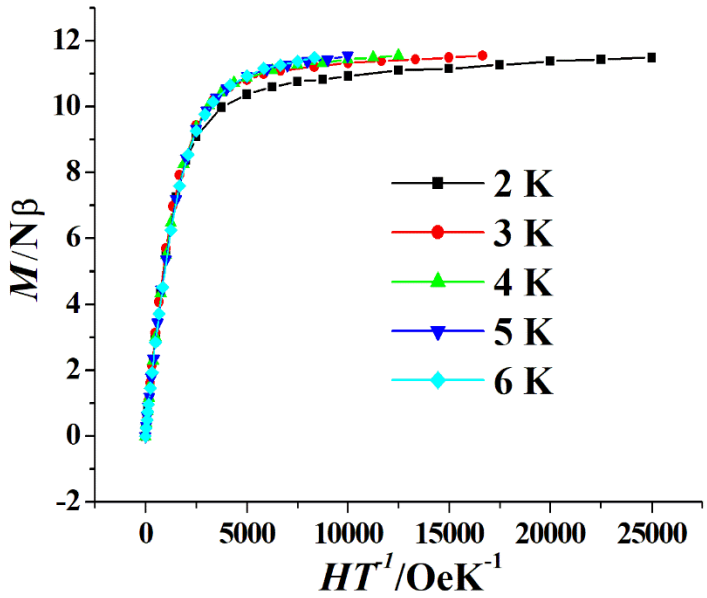

Fig. S2. *M versus H*/*T* plots at 2-6 K of *D*-**2**.

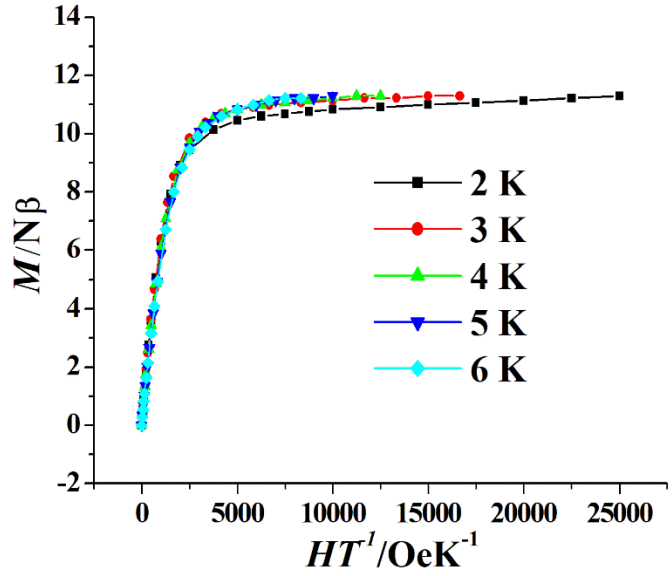

Fig. S3. *M versus H*/*T* plots at 2-6 K of *D*-**3**.

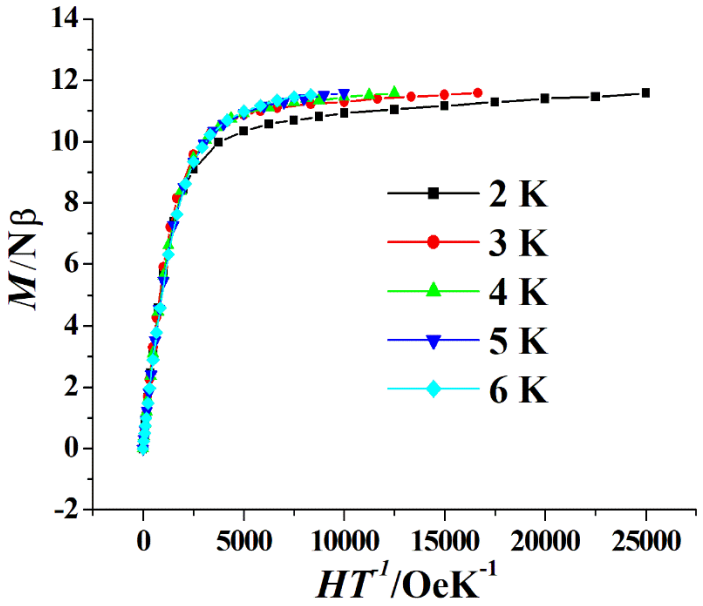

Fig. S4. *M versus H*/*T* plots at 2-6 K of *D*-**4**.

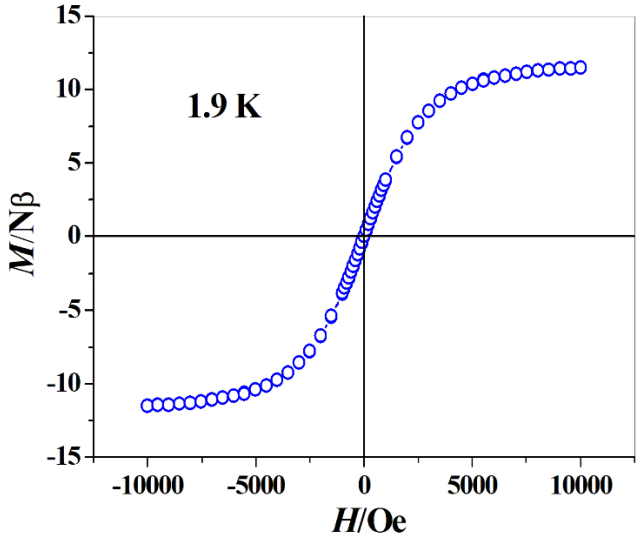

Fig. S5. Hysteresis loop for *D*-**1** at 1.9 K.

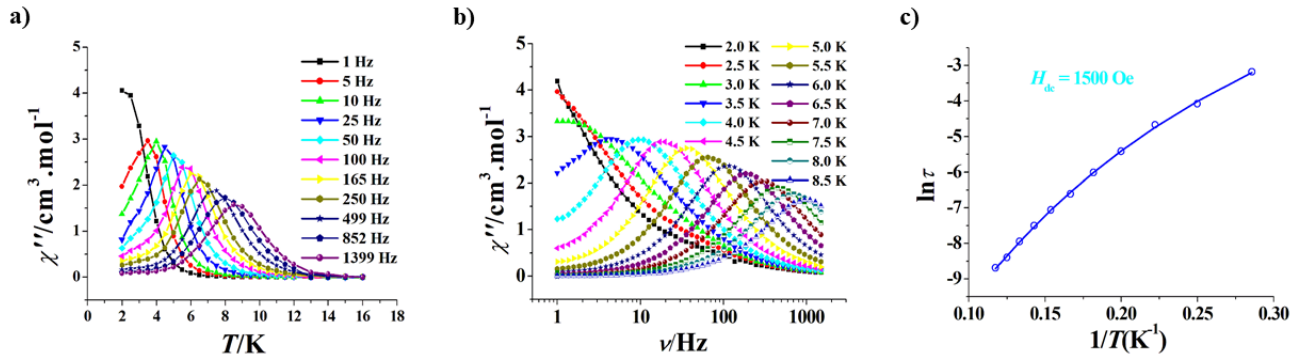

Fig. S6. Plots of χ'' *versus* T for *D*-**1** (H_{dc} = 1500 Oe) (a). Frequency dependence of χ'' for *D*-**1** at 1500 Oe (b). Plot of ln(τ) *versus* 1/T for *D*-**1** (H_{dc} = 1500 Oe), the solid line represents the best fitting with Orbach plus Raman (c).

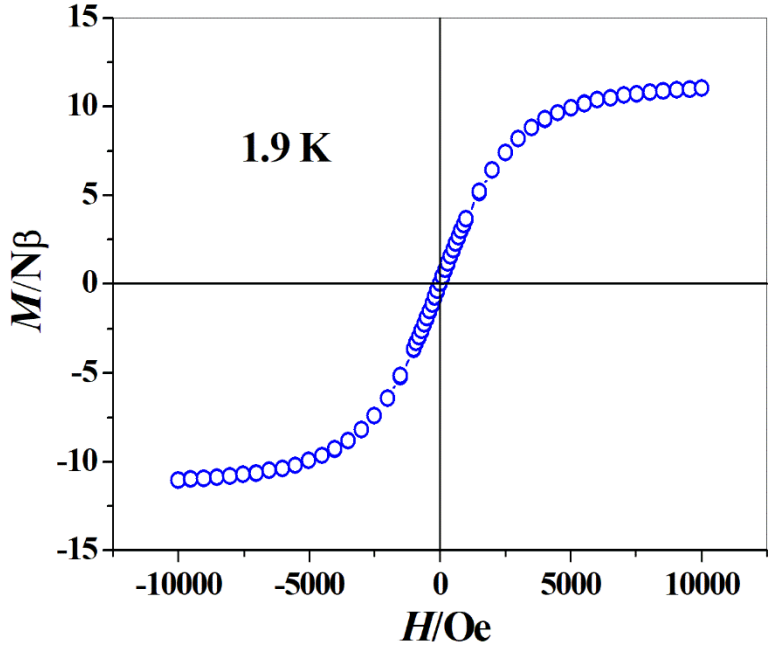

Fig. S7. Hysteresis loop for *D*-**2** at 1.9 K.

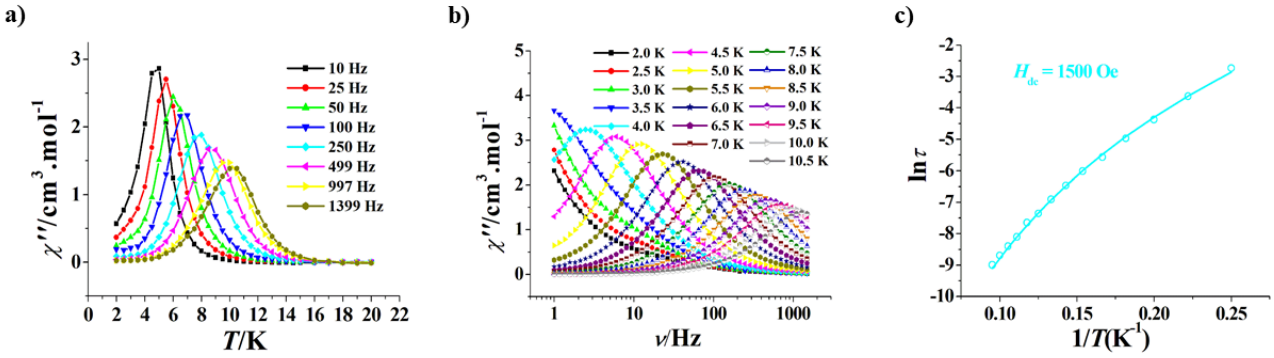

Fig. S8. Plots of χ'' *versus* T for *D*-**2** (H_{dc} = 1500 Oe) (a). Frequency dependence of χ'' for *D*-**2** at 1500 Oe (b). Plot of ln(τ) *versus* 1/T for *D*-**2** (H_{dc} = 1500 Oe), the solid line represents the best fitting with Orbach plus Raman (c).

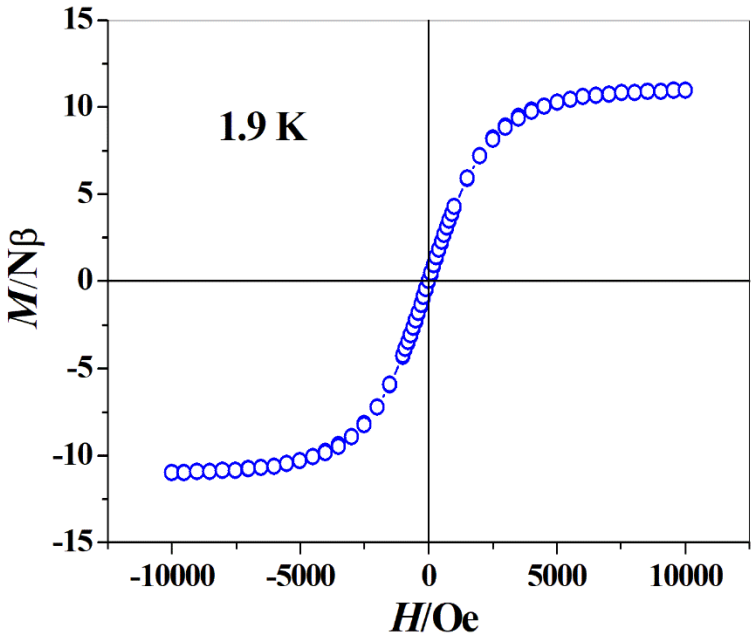

Fig. S9. Hysteresis loop for *D*-**3** at 1.9 K.

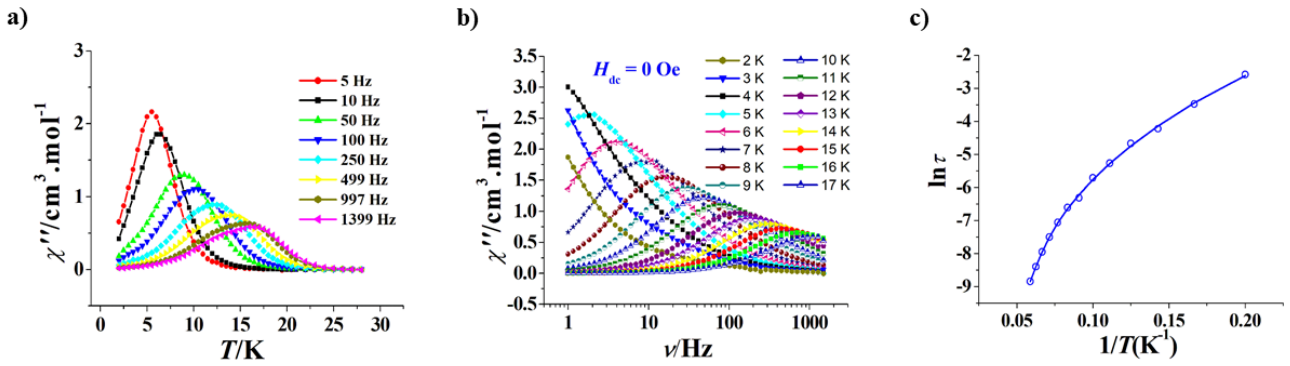

Fig. S10. Plots of χ'' *versus* T for *D*-**3** (H_{dc} = 1500 Oe) (a). Frequency dependence of χ'' for *D*-**3** at 1500 Oe (b). Plot of ln(τ) *versus* 1/T for *D*-**3** (H_{dc} = 1500 Oe), the solid line represents the best fitting with Orbach plus Raman (c).

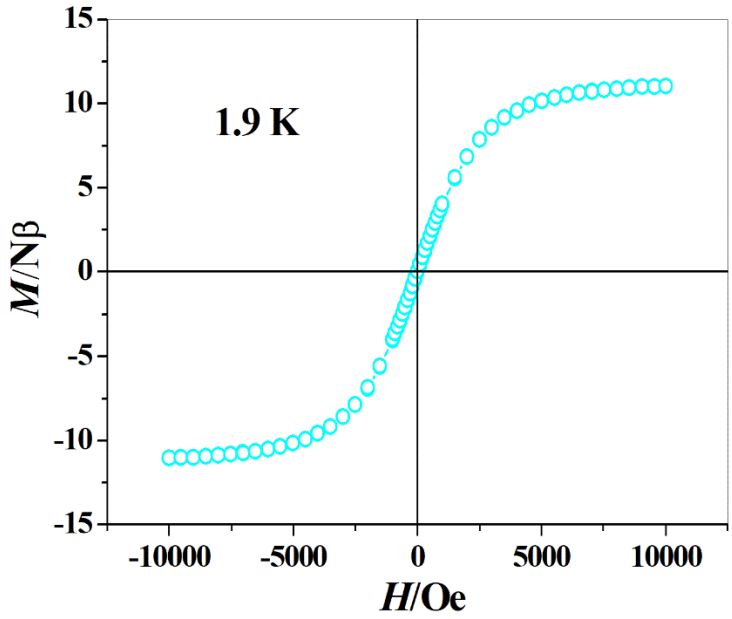

Fig. S11. Hysteresis loop for *D*-**4** at 1.9 K.

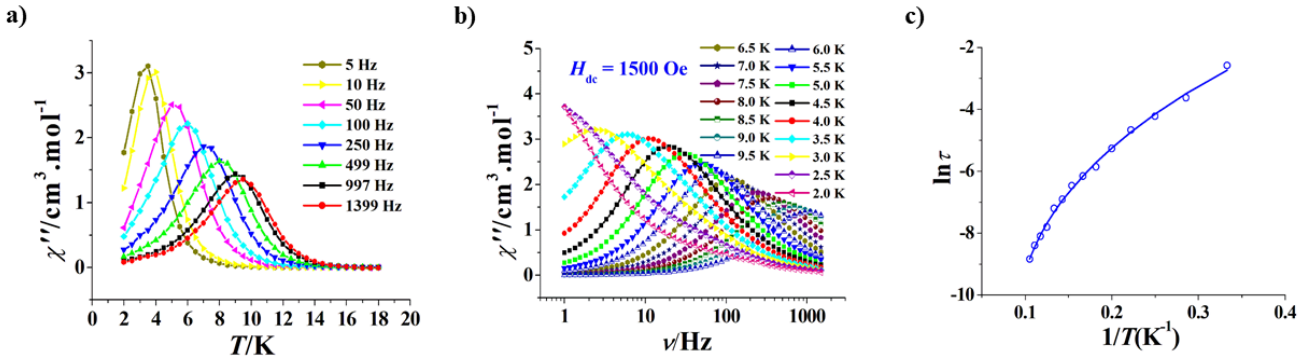

Fig. S12. Plots of χ'' *versus* T for *D*-**4** (H_{dc} = 1500 Oe) (a). Frequency dependence of χ'' for *D*-**4** at 1500 Oe (b). Plot of ln(τ) *versus* 1/T for *D*-**4** (H_{dc} = 1500 Oe), the solid line represents the best fitting with Orbach plus Raman (c).

Supporting Information for theoretical calculations

Ab initio calculations were performed with MOLCAS 8.1 program.[1] All atoms are described by relativistic atomic natural orbital (ANO) basis sets from the MOLCAS ANO-RCC library: ANO-RCC-VTZP for Dy (III) ion; VTZ for coordinated O and N; VDZ for other atoms, accounting scalar relativistic contractions. A second-order Douglas-Kroll-Hess Hamiltonian was employed. The spin-orbit coupling was handled separately through the restricted-active-space state interaction procedure (RASSI-SO). Active electrons in seven active spaces include all *f* electrons (CAS (9, 7)) of Dy (III) in the CASSCF calculation.

The intramolecular interaction between two Dy (III) ions was also calculated using theoretical method. Firstly, each Dy (III) fragment was calculated using CASSCF to obtain the corresponding magnetic properties. Then, the exchange interaction between the magnetic centers is considered within the Lines model[2], while the account of the dipole-dipole magnetic coupling is treated exactly. The Lines model is effective and has been successfully used widely in the research field of f-element single-molecule magnets. For this compound, there is only one type of *J* (Dy-Dy). The Hamiltonian is as follows,

$$\hat{H}_{exch} = -J_{total}\hat{\tilde{S}}_{Dy1}\hat{\tilde{S}}_{Dy2}$$

Where the J_{total} is the parameter of the total magnetic interaction ($J_{total} = J_{dip} + J_{exch}$) between magnetic center ions. The $\hat{\tilde{S}}_{Dy1} = \pm 1/2$ are the ground pseudospin on the Dy (III) sites. The dipolar magnetic coupling can be calculated in Ising approximation, while the exchange coupling constant was fitted through comparison of the computed and measured magnetic susceptibility and molar magnetization using the POLY_ANISO program.[3]

Table S6. Calculated energy levels (K) and g (g_x, g_y, g_z) tensors of the lowest Kramers doublets (KDs) of individual Dy(III) fragment for *D*-**1**.

KDs	Dy1		Dy2	
	E / K	*g*	*E* / K	*g*
1	0.0	0.019 0.024 19.541	0.0	0.023 0.029 19.543
2	183.6	0.193 0.213 16.634	192.2	0.095 0.111 16.548
3	374.2	1.886 2.845 12.211	363.2	9.733 7.516 3.113
4	436.3	1.168 3.142 15.323	404.8	2.129 3.964 11.844
5	509.3	3.257 5.958 9.981	488.2	4.501 6.612 9.347
6	621.7	0.286 1.346 16.056	580.8	0.728 1.127 16.968
7	712.0	0.069 1.252 17.545	697.0	0.061 0.734 18.464
8	766.5	0.349 0.802 19.056	775.5	0.162 0.413 19.342

Table S7. Calculated energy levels (K) and g (g_x, g_y, g_z) tensors of the lowest Kramers doublets (KDs) of individual Dy(III) fragment for *D*-**2**.

KDs	Dy1		Dy2	
	E / K	*g*	*E* / K	*g*
1	0.0	0.024 0.037 19.504	0.0	0.014 0.020 19.460
2	180.3	0.250 0.310 16.551	193.0	0.098 0.107 16.484
3	344.6	3.115 4.819 11.361	384.3	9.387 7.514 2.725
4	394.5	0.429 2.705 14.270	419.2	2.998 3.908 10.927
5	470.1	2.664 5.531 9.825	502.7	4.029 5.605 10.888
6	602.2	0.278 1.745 15.339	583.0	0.969 1.296 17.113
7	683.6	0.272 1.393 17.214	711.1	0.548 1.633 16.758
8	735.9	0.327 0.643 19.072	740.7	0.374 2.100 17.329

Table S8. Calculated energy levels (K) and g (g_x, g_y, g_z) tensors of the lowest Kramers doublets (KDs) of individual Dy(III) fragment for *D*-**3**.

KDs	Dy1		Dy2		Dy3		Dy4	
	E / K	g	E / K	g	E / K	g	E / K	g
1	0.0	0.007 0.010 19.679	0.0	0.003 0.005 19.641	0.0	0.006 0.009 19.691	0.0	0.006 0.012 19.485
2	294.5	0.099 0.296 16.916	294.5	0.032 0.084 16.820	304.5	0.064 0.161 16.896	252.8	0.107 0.273 16.445
3	419.4	0.210 0.607 18.284	429.5	0.182 0.364 19.145	472.1	0.580 1.483 17.207	356.7	0.243 0.743 18.380
4	498.5	0.998 4.254 11.017	519.8	1.350 1.581 12.469	533.6	0.818 4.336 11.894	431.8	0.843 2.099 14.541
5	532.1	0.501 4.115 12.213	577.4	0.164 2.918 10.674	582.0	1.681 4.046 8.333	505.0	0.316 3.453 9.222
6	601.6	2.800 3.554 10.470	660.4	4.968 5.471 8.243	681.8	2.475 6.196 11.742	593.3	7.489 7.151 3.723
7	688.5	2.821 4.631 11.148	701.6	1.709 1.980 15.113	708.4	1.240 3.760 10.484	634.8	1.546 2.266 16.608
8	774.4	0.665 1.950 17.893	764.4	0.745 1.060 17.931	776.1	0.726 1.555 17.993	660.9	1.050 1.300 16.866

Table S9. Calculated energy levels (K) and g (g_x, g_y, g_z) tensors of the lowest Kramers doublets (KDs) of individual Dy(III) fragment for *D*-**4**.

KDs	Dy1		Dy2	
	E / K	*g*	*E* / K	*g*
1	0.0	0.006 0.029 19.454	0.0	0.001 0.016 19.532
2	161.0	0.163 0.238 16.575	174.5	0.194 0.249 16.674
3	314.0	10.126 7.358 3.178	367.5	2.863 4.567 11.503
4	347.8	1.823 3.767 12.664	426.8	0.511 3.423 14.697
5	432.5	3.859 6.354 9.369	510.6	3.834 6.194 9.615
6	506.5	1.461 1.902 16.543	620.2	0.731 1.638 15.657
7	656.4	0.445 0.622 18.447	724.3	11.030 6.506 1.556
8	713.7	0.252 0.961 18.679	745.7	12.466 7.569 1.046

Table S10.Wave functions with definite projection of the total moment | m_J > for the lowest three Kramers doublets (KDs) of individual Dy^{3+} fragments in *D*-**1**.

	E / K	wave functions
Dy1	0.0	95.4%|±15/2>
	183.6	88.4%|±13/2>+4.7%|±7/2>
	374.2	64.8%|±11/2>+6.9%|±9/2>+8.0%|±3/2>+8.8%|±1/2>
Dy2	0.0	95.7%|±15/2>
	192.2	88.2%|±13/2>+4.8%|±7/2>
	363.2	54.2%|±11/2>+9.7%|±9/2>+14.5%|±3/2>+10.5%|±1/2>

Table S11. Wave functions with definite projection of the total moment | m_J > for the lowest three Kramers doublets (KDs) of individual Dy^{3+} fragments in *D*-**2**.

	E / K	wave functions
Dy1	0.0	95.3%|±15/2>
	180.3	84.5%|±13/2>+4.7%|±11/2>+4.4%|±7/2>
	344.6	45.7%|±11/2>+10.0%|±9/2>+4.6%|±7/2>+16.3%|±3/2>+17.9%|±1/2>
Dy2	0.0	93.5%|±15/2>
	192.2	88.8%|±13/2>+3.5%|±9/2>+4.7%|±7/2>
	363.2	48.2%|±11/2>+8.4%|±9/2>+6.3%|±7/2>+15.6%|±3/2>+14.5%|±1/2>

Table S12. Wave functions with definite projection of the total moment | m_J > for the lowest three Kramers doublets (KDs) of individual Dy^{3+} fragments in *D*-**3**.

	E / K	wave functions
Dy1	0.0	97.0%|±15/2>
	294.5	80.0%|±13/2>+8.3%|±11/2>+7.6%|±9/2>
	419.4	41.6%|±1/2>+33.3%|±3/2>+16.3%|±5/2>+4.5%|±7/2>
Dy2	0.0	95.8%|±15/2>
	294.5	80.9%|±13/2>+5.4%|±11/2>+9.2%|±9/2>
	429.5	29.7%|±1/2>+29.8%|±3/2>+22.8%|±5/2>+11.0%|±7/2>+4.0%|±9/2>
Dy3	0.0	96.2%|±15/2>
	304.5	82.5%|±13/2>+6.5%|±11/2>+7.9%|±9/2>
	472.1	52.6%|±1/2>+28.6%|±3/2>+7.7%|±5/2>+4.6%|±7/2>
Dy4	0.0	93.6%|±15/2>
	294.5	83.4%|±13/2>+9.3%|±11/2>+3.5%|±9/2>
	429.5	45.4%|±1/2>+30.1%|±3/2>+14.9%|±5/2>+6.0%|±7/2>+1.1%|±9/2>

Table S13. Wave functions with definite projection of the total moment | m_J > for the lowest three Kramers doublets (KDs) of individual Dy^{3+} fragments in *D*-**4**.

	E / K	wave functions
Dy1	0.0	94.5%|±15/2>
	161.0	81.5%|±13/2>+7.5%|±11/2>+5.4%|7/2>
	314.0	44.8%|±11/2>+17.8%|±9/2>+17.0%|±3/2>+10.4%|±1/2>
Dy2	0.0	95.1%|±15/2>
	174.5	86.5%|±13/2>+4.6%|±11/2>+4.5%|7/2>
	363.2	59.8%|±11/2>+8.1%|±9/2>+10.8%|±3/2>+7.5%|±1/2>

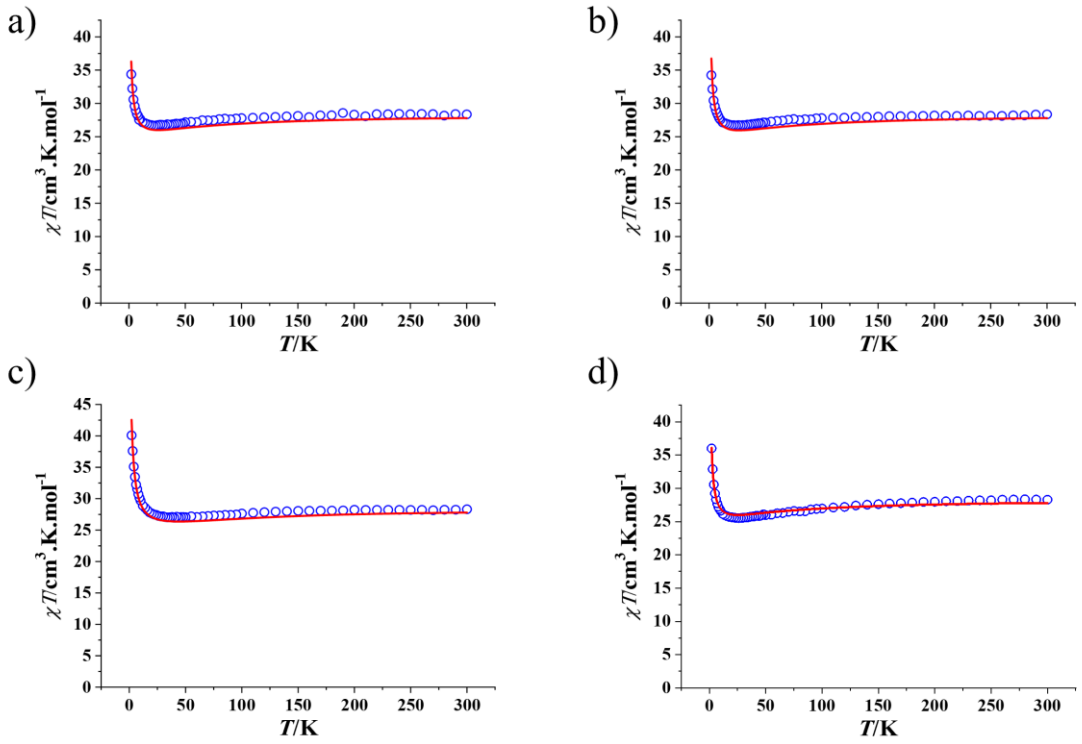

Fig. S13. Plot of χT *versus* T of *D*-**1** (H_{dc} = 1000 Oe) (a); Plot of χT *versus* T of *D*-**2** (H_{dc} = 1000 Oe) (b); Plot of χT *versus* T of *D*-**3** (H_{dc} = 1000 Oe), and the simulated results are obtained from Dy1 and Dy2. (c); Plot of χT *versus* T of *D*-**4** (H_{dc} = 1000 Oe) (d);The red line corresponds to the simulated results.

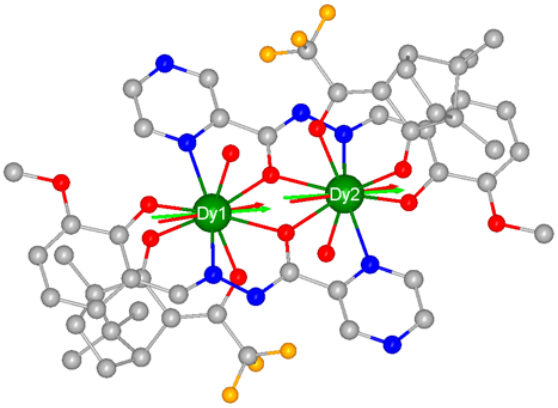

Fig. S14. The orientations of easy axis of the KDs on Dy^{3+} for *D*-**1**. The green arrow represents the ground KDs and the red stands for the first excited KDs. Color codes: Dy, green; N, blue; O, red; C, grey; F, light orange. All hydrogens are omitted for clarity.

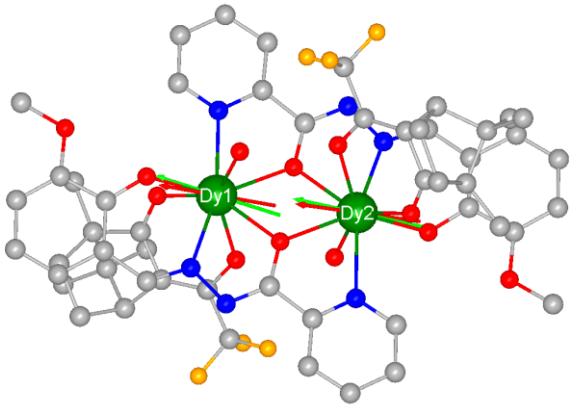

Fig. S15. The orientations of easy axis of the KDs on Dy^{3+} for *D*-**2**. The green arrow represents the ground KDs and the red stands for the first excited KDs. Color codes: Dy, green; N, blue; O, red; C, grey; F, light orange. All hydrogens are omitted for clarity.

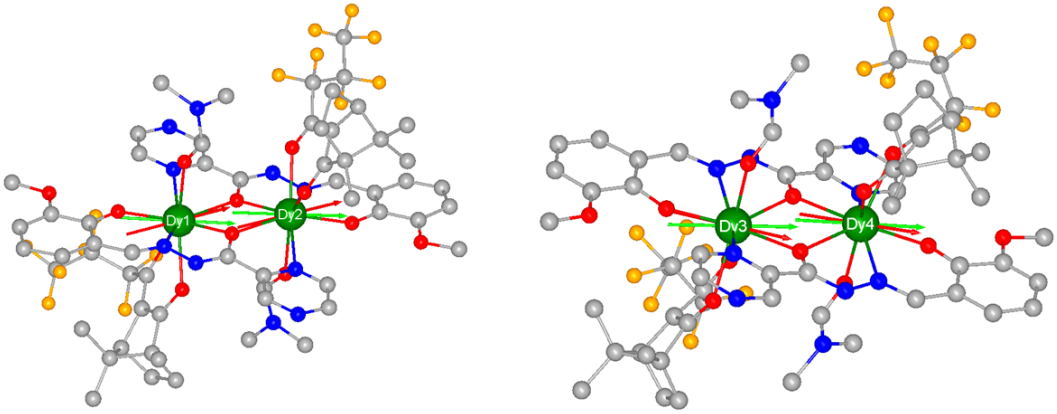

Fig. S16. The orientations of easy axis of the KDs on Dy^{3+} for *D*-**3**. The green arrow represents the ground KDs and the red stands for the first excited KDs. Color codes: Dy, green; N, blue; O, red; C, grey; F, light orange. All hydrogens are omitted for clarity.

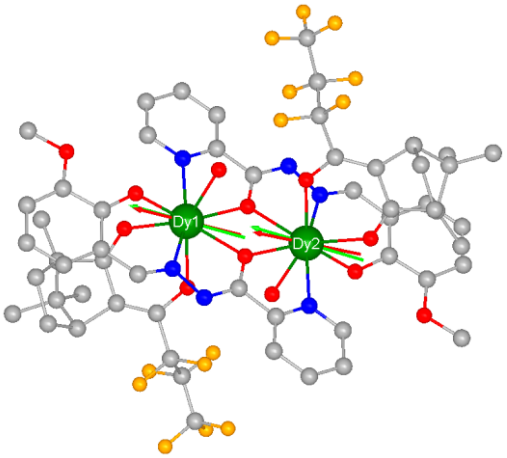

Fig. S17. The orientations of easy axis of the KDs on Dy^{3+} for *D*-**4**. The green arrow represents the ground KDs and the red stands for the first excited KDs. Color codes: Dy, green; N, blue; O, red; C, grey; F, light orange. All hydrogens are omitted for clarity.

References:

(1) Aquilante, F.; Autschbach, J.; Carlson, R. K.; Chibotaru, L. F.; Delcey, M. G.; Vico, L. D.; Galván, I. F.; Ferré, N.; Frutos, L. M.; Gagliardi, L.; Garavelli, M.; Giussani, A.; Hoyer, C. E.; Manni, G. L.; Lischka, H.; Ma, D.; Malmqvist, P. Å.; Müller, T.; Nenov, A.; Olivucci, M.; Pedersen, T. B.; Peng, D.; Plasser, F.; Pritchard, B.; Reiher, M.; Rivalta, I.; Schapiro, I.; Segarra-Martí, J.; Stenrup, M.; Truhlar, D. G.; Ungur, L.; Valentini, A.; Vancoillie, S.; Veryazov, V.; Vysotskiy, V. P.; Weingart, O.; Zapata, F.; Lindh, R. Molcas 8: New capabilities for multiconfigurational quantum chemical calculations across the periodic table. *J. Comput. Chem.* **2016**, *37*, 506.

(2) Lines, M. E. Orbital Angular Momentum in the Theory of Paramagnetic Clusters. *J. Chem. Phys*. **1971**, *55*, 2977.

(3) (a) Chibotaru, L. F.; Ungur, L.; Soncini, A. Origin of non-magnetic Kramers doublets in the ground state of dysprosium triangles: Evidence for toroidal magnetic moment. *Angew. Chem. Int. Ed.* **2008**, *47*, 4126; (b) Chibotaru, L. F.; Ungur, L.; Aronica, C.; Elmoll, H.; Pilet, G.; Luneau, D. Structure, magnetism and theoretical study of mixed-valent $Co^{II}_3Co^{III}_4$ heptanuclear wheel: Lack of SMM behaviour despite negative magnetic anisotropy. *J. Am. Chem. Soc.* **2008**, *130*, 12445.

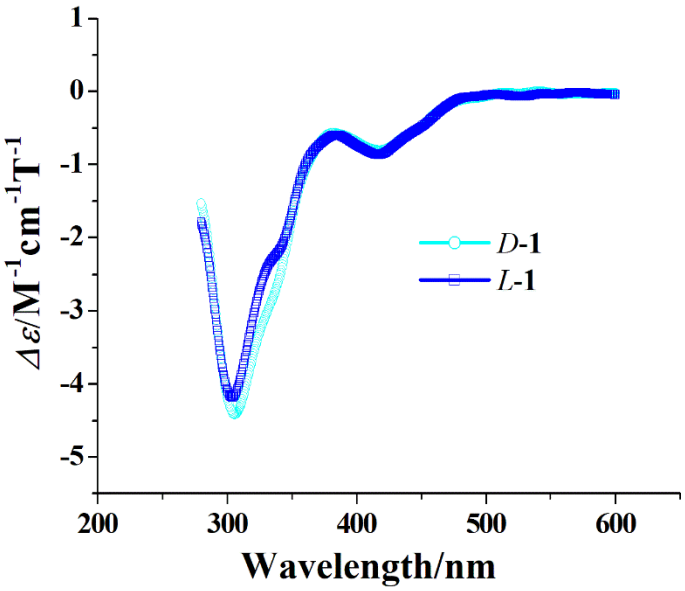

Fig. S18. MCD spectra of *D*-**1** and *L*-**1**.

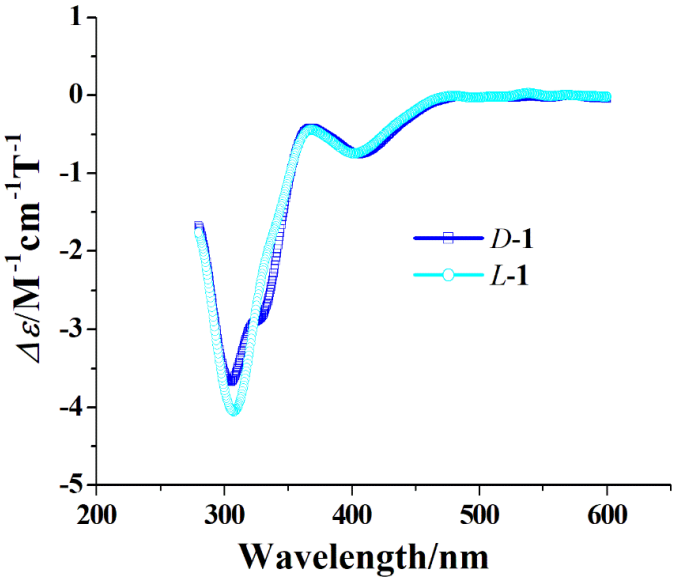

Fig. S19. MCD spectra of *D*-**2** and *L*-**2**.

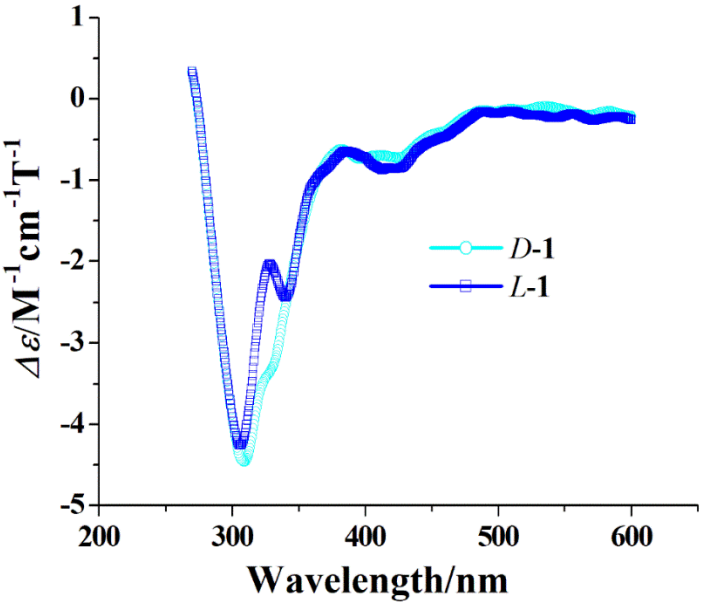

Fig. S20. MCD spectra of *D*-**3** and *L*-**3**.

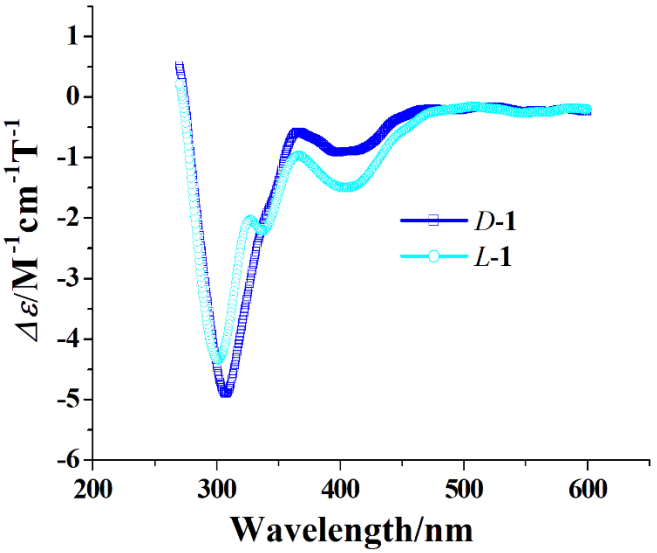

Fig. S21. MCD spectra of *D*-**4** and *L*-**4**.

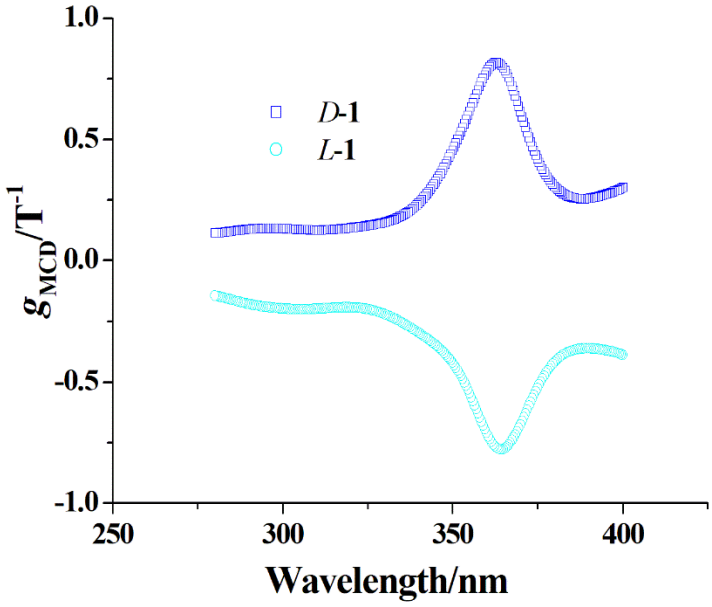

Fig. S22. The wavelength-dependent g_{MCD} of *D*-**1** and *L*-**1**.

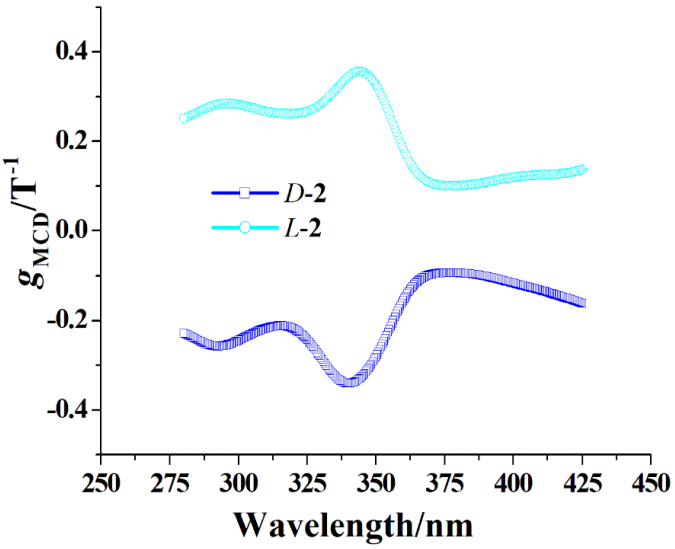

Fig. S23. The wavelength-dependent g_{MCD} of *D*-**2** and *L*-**2**.

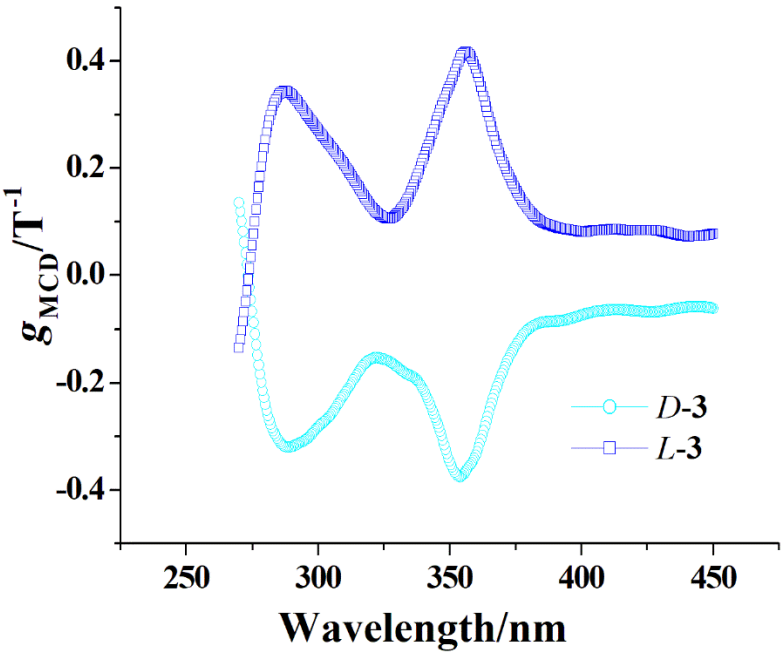

Fig. S24. The wavelength-dependent g_{MCD} of *D*-**3** and *L*-**3**.

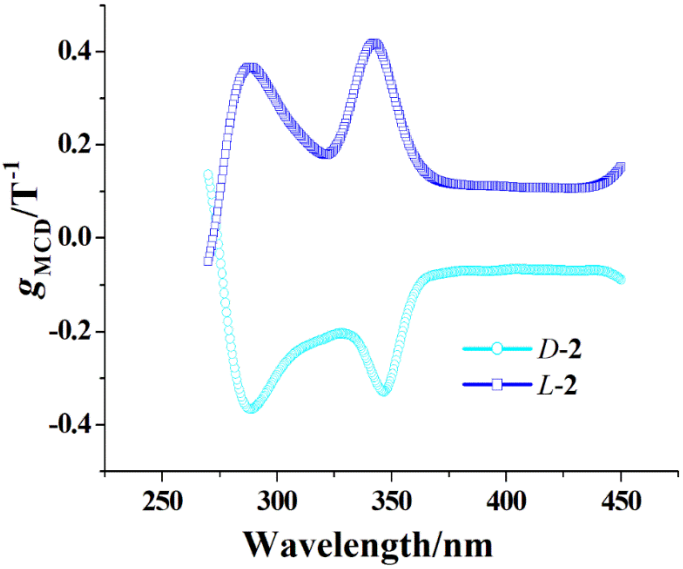

Fig. S25. The wavelength-dependent g_{MCD} of *D*-**4** and *L*-**4**.

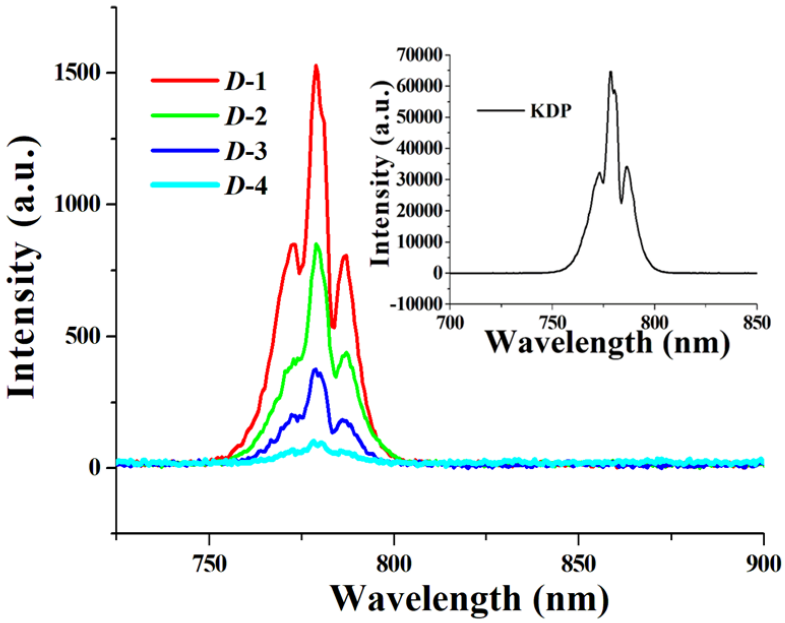

Fig. S26. SHG spectra of crystalline samples of *D*-**1**, *D*-**2**, *D*-**3**, *D*-**4** and KDP (illustration) under excitation at λ = 1550 nm (T_{int} = 0.5 s).